Layout: T1 Standard SC | Series ID: 8415 | MS No.: vol07mcgloughlin08figueroa
Chapter No.: 73 | Date: 4-4-2011 | Page: 1/26

Computational Analysis of Displacement Forces Acting on Endografts Used to Treat Aortic Aneurysms

C. Alberto Figueroa and Christopher K. Zarins

Abstract Endovascular repair has greatly reduced the perioperative morbidity and mortality of abdominal aortic aneurysm repair compared to open surgery (Zarins et al., J Vasc Surg 38(6): 1264–1272, 2003). However, endovascular stent-grafts are exposed to a number of clinical complications, such as endograft migration (i.e., loss of positional stability), stent fractures and endoleaks (i.e., persistence of blood flow into the aneurysm sac after device placement). These complications may result in life-threatening and costly events such as aneurysm growth, rupture, need for secondary procedures, and life-long follow-up with imaging studies. Understanding the biomechanical environment experienced by endografts in vivo is a critical factor in improving their performance (Figueroa et al., J Endovasc Ther 16(3):350–358, 2009; 284–294, 2009). The loads experienced by aortic endografts are greatly dependent on the tortuosity and size of the endograft, as well as on the hemodynamic state of the patient. The fixation response of the endograft is determined by factors such as the fixation mechanism (radial pressure vs. hooks and barbs), amount of "landing zone" (i.e., area where the endograft can physically attach to the aorta), and the disease state of the vessel wall at the landing zone. The purpose of this study is to review the most common complications associated with endovascular repair of abdominal and thoracic aneurysms, and to provide a summary of the state of the art of the computational tools used to perform patient-specific modeling of endograft dynamics.

C. Alberto Figueroa (✉)
Department of Bioengineering, Stanford University, Stanford, CA, USA
e-mail: cafa@stanford.edu

C. K. Zarins
Department of Surgery, Stanford University, Stanford, CA, USA
e-mail: zarins@stanford.edu

Stud Mechanobiol Tissue Eng Biomater
DOI: 10.1007/8415_2011_73

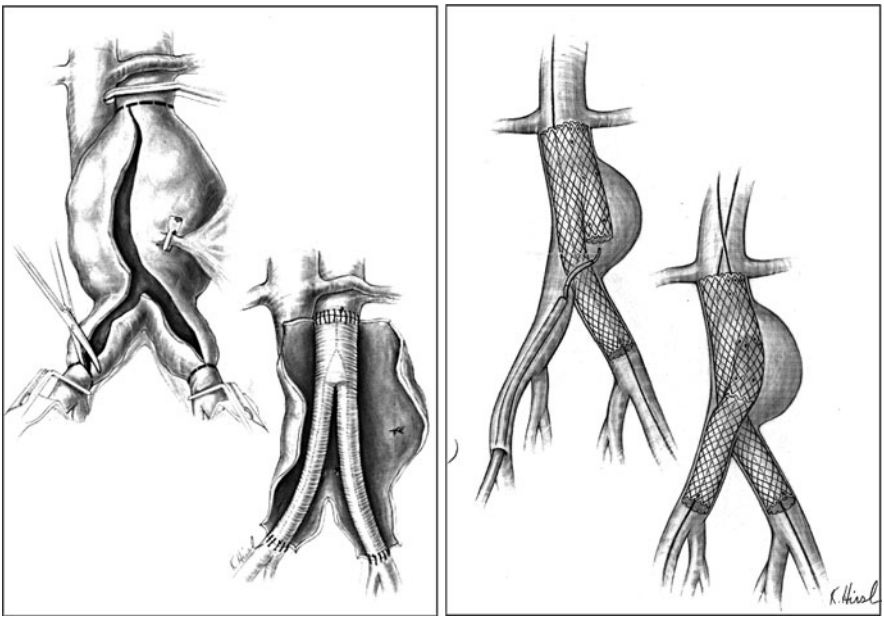

Fig. 1 Left In an open surgical AAA repair, a Dacron graft is manually sutured to the aortic neck and common iliac arteries.Right In an endovascular repair, a stent-graft is deployed in the aneurysm cavity using a catheter. Adapted from Zarins and Gewertz [49]

1 Introduction

The prevalence of abdominal aortic aneurysms (AAA) has increased 300% over the past 40 years. Currently, aneurysm disease affects 5–7% of Americans over age 60 and the number of aneurysms is expected to increase dramatically in the next years as the population ages [12, 14]. Abdominal aneurysms can be repaired using open surgery or endovascular techniques.

1.1 Open Repair

In this procedure, a large transperitoneal or retroperitoneal incision is made to expose the diseased section of the aorta. Then, the aortic neck and iliac arteries are clamped to temporarily interrupt blood flow into the aneurysm. The aneurysmal aorta is cut open and the intraluminal thrombus is removed. A Dacron or PTFE graft is anastomosed to the infrarenal aorta and common iliac arteries (see Fig.1) and the thrombus-free aneurysm wall is closed over the graft [49]. This procedure usually requires a 3–5 h long operation, which is physiologically stressful for

the patient. Despite the numerous technological advances and improvement in perioperative management advances during the last 55 years of clinical practice, this approach is still associated with significant operative mortality rates (5 and 50% for elective and ruptured repairs, respectively) [7, 18].

1.2 Endovascular Repair

Endovascular repair techniques have revolutionized the treatment of AAA disease, greatly reducing the perioperative mortality and morbidity associated with open surgical repair [5]. These techniques were first introduced in 1990 by Juan Parodi [32] using a home-made device consisting of a modified Palmaz stent sutured to a Dacron vascular graft to exclude an abdominal aneurysm. The stent-graft is deployed in the abdominal aortic region using a catheter guided fluoroscopically. Once deployed, the stent-graft forms a new conduit for the blood, effectively excluding the weakened aneurysm wall from the direct action of blood pressure. The technique requires only small incisions in the groin to expose the femoral artery and thus is a safer procedure for the patient than open repair. Endovascular aneurysm repair has experienced rapid development and wide acceptance during the last decade and has become the primary treatment for AAA disease in the USA [15]. While initially the technique was used primarily in older patients who could not tolerate the risk ofi nvasive open repair, endovascular repair is now used to treat a broad range of patients and aneurysm morphologies [8, 16]. This has been possible due to the evolution in design and fixation characteristics of endografts through the years. Most modern devices include supra-renal fixation that enables the use of the device in patients with short aortic necks or with aneurysms that extend close to the renal arteries. There are currently multiple devices in the market that are very different in design (modular vs. unibody), materials (Dacron vs. PTFE; nitinol vs. stainless steel or cobalt-chromium), deployment mechanisms (self-expanded vs. balloon-expanded) and attachment mechanisms (radial force vs. hooks & barbs), (see Fig. 2).

Despite the aforementioned advantages, endovascular aneurysm repair is not free of significant complications, such as late endograft migration (see Fig. 3), endoleak formation, fracture of device components, etc. that may result in continued aneurysm expansion and the need for long-term imaging surveillance and secondary interventions. Furthermore, the EVAR-1 clinical trial showed that hospital costs are higher for patients treated with endovascular repair than for those treated with open repair [16].

Recent data from the DREAM prospective randomized clinical trial comparing long-term outcomes of aneurysm repair in patients treated with open and endovascular techniques indicates that re-intervention rates are significantly smaller in the open repair group with similar survival rates after 7 years [8]. It is therefore fair to say that while endovascular procedures greatly reduce the problems that

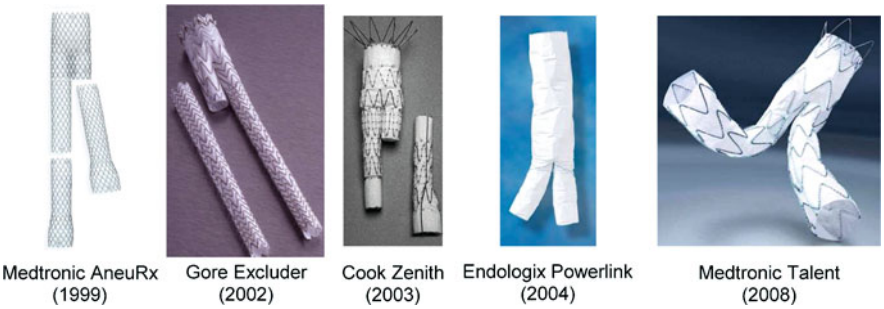

Fig. 2 Current FDA approved endografts for abdominal aortic aneurysm repair. Year of FDA approval is listed in parenthesis

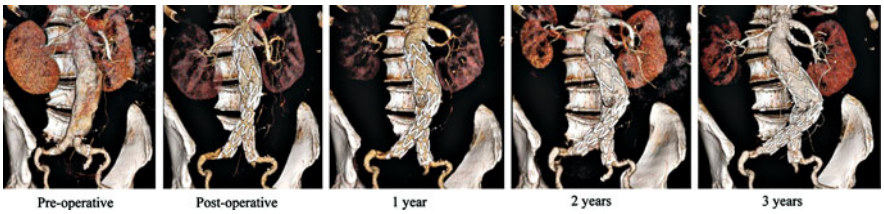

Fig. 3 Medical image follow-up studies of an abdominal aortic aneurysm repaired using a stent-graft. The images show the pre-operative, post-operative and several follow-up configurations of the abdominal aorta and the endograft, clearly demonstrating the migration of the device. The patient eventually required a secondary procedure where a proximal extender cuffwas placed in the aortic neck

open repair originates in the short-term; they generate a number of drawbacks that negatively impact the long-term well-being of the patient. It is thus of critical importance to enhance the performance of endografts by improving their design based on a deeper understanding of the hemodynamic conditions that the devices experience in vivo.

2 Endograft Failure Modes

The most common post-operative complications in endovascular repair are endoleaks (i.e., persistence of blood flow into the aneurysm sac after device placement) and endograft migration (i.e., loss of positional stability). Other modes of failure are graft rupture, infection or thrombosis; and endotension (i.e., continuous aneurysm sac expansion in the absence of endoleaks).

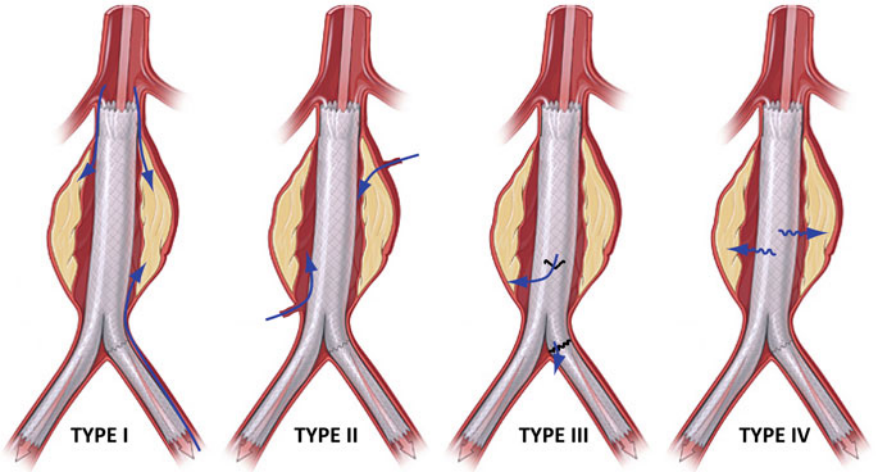

Fig. 4 Schematic representation of the endoleak types following AAA endovascular repair

2.1 Endoleaks

Endoleaks are present in 20–40% of patients following endovascular aneurysm repair. Endoleaks are considered to be dangerous because in their presence, the intra-saccular pressure remains elevated and therefore the risk of rupture of the aneurysm persists. Endoleaks can be classified according to their temporal nature (i.e., short-term or long-term) or to the origin of the endoleak [46] (see Fig. 4):

- Type I endoleaks are the result of poor apposition of the device to the aortic wall. Type Ia refers to blood flow coming into the aneurysm sac from the proximal fixation area, whereas Type Ib refers to flow coming into the aneurysm from the distal fixation zone. Type I endoleaks are considered to be evidence of a poorly performed procedure. They usually account for less than 10% of all endoleak cases [42].
- Type II endoleaks occur when there is reverse flow into the aneurysm sac from aortic branch vessels such as the inferior mesenteric artery or lumbar arteries. This is the most common type of endoleak, accounting for more than half of the cases. Some Type II endoleaks thrombose spontaneously shortly after the procedure. Others persist, and may lead to aneurysm enlargement. If the physician determines that these persistent Type II endoleaks represent a threat, they are treated by coil embolization of the arteries responsible for the retrograde flow [3].
- Type III endoleaks may be due to a defect in the fabric of the graft, such as a tear resulting from a fractured stent, or due to separation of the modular components of the endograft. These endoleaks usually account for less than 5% of the cases.

- Type IV endoleaks are due to filtration of plasma through the fabric of the graft. This is usually the result of a design feature of the graft fabric.

2.2 Endograft Migration

All endografts are subject to migration as a result of the pulsatile action of blood flow and pressure. Endograft migration represents a serious adverse event that usually requires a secondary intervention to restore proper fixation of the device to the abdominal aorta. This secondary procedure may involve the insertion of a proximal or distal extender cuffdeployed endovascularly, or open surgical repair procedures such as aortic neck plication and partial or complete endograft removal [31].

To date, there has not been a consistent definition of endograft migration. Some device manufacturers have defined migration as a proximal or distal endograft movement more than 5 mm, whereas others set the threshold at 10 mm. Furthermore, the term migration has often referred to situations where endograft movement results in a clinical event. Under this definition, numerous cases of significant endograft movement that do not result in an adverse clinical event are not regarded as migration [11]. Therefore, the concept of positional stability may be understood differently in clinical and engineering settings.

There are multiple clinical studies that have examined the rates of migration of various devices over time. In general, migration rates increase over time for all devices [27, 40, 48]. These studies have examined the proximal and distal motion of the endograft, but they have neglected the sideways motion. This sideways component has been recently shown to be a predictor of endograft migration and late adverse events [33].

Most current endograft designs rely on two different mechanisms to fixate the device to the arterial wall: radial force and hooks or barbs (see Fig. 5). In the case of radial force, this is achieved by oversizing the device relative to the nominal aortic diameter. The larger the oversizing of the device, the larger the radial force developed against the wall and therefore the larger the fixation response of the device. The degree of oversizing in clinical practice varies significantly, ranging from as little as 5% to as large as 30%. Aortic neck dilation and Type Ia endoleaks have been associated with excessive device oversizing [6, 39, 40, 48]. This is perhaps due to remodeling in the vessel wall in response to the larger circumferential stresses originated by excessive device oversizing. In the case of hooks and barbs, these components penetrate the vessel wall, thus clamping the device to the arterial lumen. A basic design parameter is the length of the hooks and barbs: the longer the hooks, the deeper the penetration through the aortic wall. However, a possible downside of this fixation approach may be the injury that these components cause to the endothelial and intima layers. This may result in vessel wall remodeling that can potentially lead to aortic neck dilation and Type Ia endoleaks.

Fig. 5 The attachment of the endograft to the aortic neck wall is achieved via radial force created by device oversizing (left) or hooks and barbs that clamp the device to the arterial lumen (right)

A number off actors which may affect device migration have been clinically investigated including aortic neck diameter [37], length and angulation [13, 19], neck calcification and thrombus, inadequate proximal and distal fixation length [17], [48] and aneurysm tortuosity [39]. In general, it has been found that longer, disease-free aortic necks are associated with lower incidence of endoleaks and endograft migration since they offer a better surface for the device to stay attached to the arterial wall. Conversely, short, calcified, tortuous necks are associated with a higher incidence of endograft complications.

In addition to the aforementioned clinical studies, experimental in vitro, in vivo, and cadaveric aorta studies have measured the pull-out forces of different devices [2, 25, 30, 35]. In all cases, these experiments considered a rather unrealistic planar configuration of the abdominal aorta and the endograft, in part due to the difficulty of reproducing an anatomically and hemodynamically-realistic experimental environment. In all these studies, the stent-graft was displaced by applying a force in the downwards direction (see Fig. 6), and the amount of force required to dislodge the endograft was recorded. This force is known as displacement force (DF).

The range of measured displacement forces for various devices was (4–30) Newton (N). These investigations are fundamentally limited because their experimental conditions fail to reproduce critical components that define the in

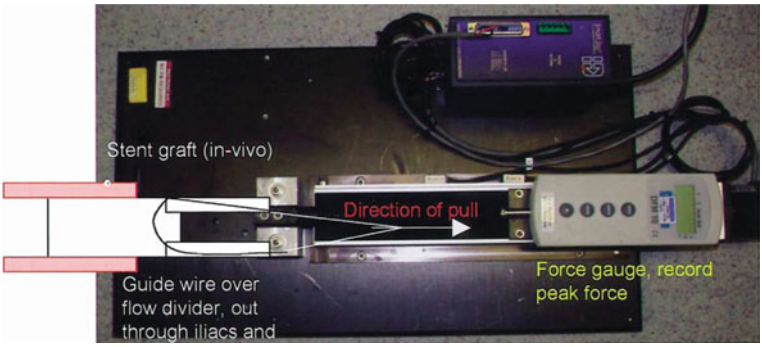

Fig. 6 Experimental setup to measure the pull-out force required to dislodge an endograft inserted in a bovine AAA model. Note the downwards direction of pull, reproduced from Arko et al. [2]

vivo hemodynamics experienced by the endograft, such as tortuous anatomy, curvature, and pulsatile flow and pressure. These conditions can potentially be better investigated with the help of computational modeling techniques.

3 CFD Modeling Tools for Endograft Dynamics

Computational modeling tools provide an opportunity to evaluate multiple situations where it is extremely difficult to generate an experimental setup that adequately reproduces the environment conditions of the problem at hand. In our case, in order to understand the principles that govern endograft stability, one must be able to reproduce realistic geometries, flow and pressure pulsatile conditions, and material properties of the components in the system. From a mechanical standpoint, the problem of endograft positional stability can be regarded as a competition between de-stabilizing forces or loads acting on the device (i.e., the displacement forces DF) and stabilizing forces that keep the device attached to the wall (i.e., fixation forces FF), see Fig. 7.

The displacement force DF is determined by the endograft geometry (i.e., length, diameter, etc.), the hemodynamic state of the patient (i.e., hypertension, cardiac output, etc.) and the anatomy of the aneurysm (i.e., tortuosity, neck angulation, etc.). The fixation forces FF must balance the displacement forces DF to keep the device attached to the vessel wall. The FF depends on the specific endograft fixation mechanism (i.e., radial force versus hooks and barbs), the structural stiffness of the device, the amount of proximal and distal landing zone (i.e., "fixation real estate"), and the level of disease of the vessel wall in the attachment areas (i.e., healthy wall versus atherosclerotic wall, presence of calcifications, etc.). The larger the loads exerted by the blood on the device, the larger

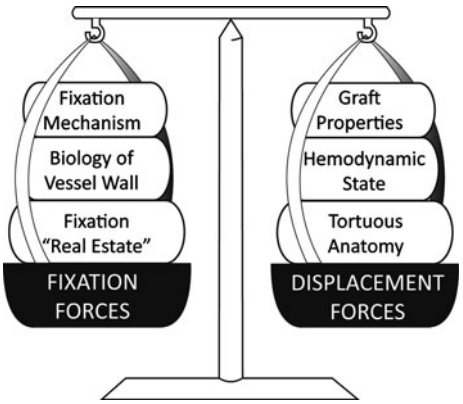

Fig. 7 The problem of endograft long-term durability seen as a competition of de-stabilizing forces or loads acting on the device (displacement forces DF) and stabilizing forces (fixation forces FF)

the fixation forces required in order to keep the device in place. Computational fluid dynamics (CFD) tools can be used to evaluate the displacement forces that the fluid (blood) exerts on the device. Likewise, computational solid mechanics (CSM) can be used to estimate the fixation forces FF that the device develops to counteract the actions of blood flow and pressure. It is therefore of critical importance to have a good understanding of the magnitude of the loads that the endograft experiences in vivo in order to ensure a design that will guarantee the long-term stability of the device.

Numerous CFD and theoretical analyses have investigated the magnitude of the DF loads exerted by blood flow on endografts using simplified computational models and boundary conditions [20, 24, 28, 29]. In most of these computational models, the geometry utilized was a simple bifurcated graft not including any of the abdominal blood vessels, usually in a planar configuration, and with simplistic outflow boundary conditions such as prescribed pressure waves in the outlet faces. Lastly, almost no studies have investigated the contact mechanics problem between the endograft and vessel wall [1]. In this setting, a 3-body contact problem involving the aortic wall, the stent, and the graft subjected to the CFD DF seeks to investigate the positional stability of the stent-graft. There are 3 possible outcomes in this stability analysis:

- The device and the aortic wall remain attached to each other. This situation corresponds to a stable endograft.
- There is slip between the endograft and the aortic wall surface. This corresponds to a situation of endograft positional instability and possible migration.
- There is separation between the endograft and the aortic wall surfaces. This corresponds to a situation of an endoleak.

In the remainder of this chapter, we review several CFD tools we have used to characterize displacement forces acting on anatomically-realistic models of aortic endografts under physiologically-relevant flow and pressure conditions.

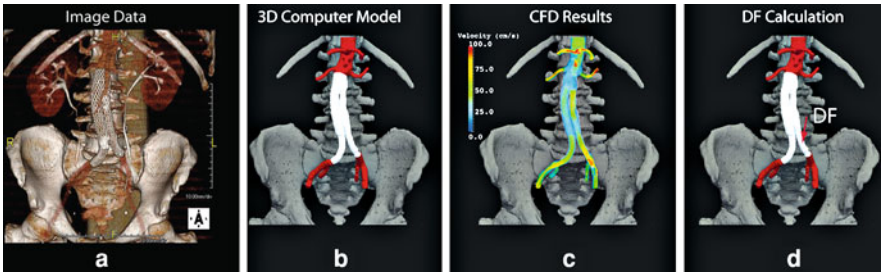

Fig. 8 Patient-specific computer modeling for displacement force calculation: Starting with the patient image data (A), 3D computer models of the endograft and the abdominal aorta are built (B). Then, CFD analyses calculating blood flow velocity and pressure in the computer model are performed (C). Lastly, the displacement force is computed using the results of the CFD analysis (D). Reproduced from Figueroa et al. [11]

3.1 Computational Fluid Dynamics Tools

The computation of DF in realistic models of aortic endografts under realistic conditions of flow and pressure relies on the so-called patient-specific computer modeling paradigm [41] (see Fig. 8). Here, a computer model of the aorta and endograft is built from medical image data using automatic segmentation techniques. Once the model is adequately discretized into a grid suitable for numerical computation, and adequate boundary conditions are applied to the model, a computer simulation representing blood flow and pressure in the domain of interest is obtained. At this point, the CFD results can be used to investigate specific quantities of interest, such as the overall displacement force exerted by blood flow on the endograft.

3.1.1 Geometric Modeling

Patient-specific geometric models of blood vessels have been constructed using 2 or 3D-based semi-automatic segmentation techniques [45, 47]. These techniques use algorithms such as the level set method to detect the lumen boundary [26]. 2D-based techniques provide higher control in the segmentation process especially in situations of significant noise in the image data, but 3D techniques are better suited to handle complex geometrical features, such as bifurcations and irregular surfaces. Contrast-enhanced medical image data such as Magnetic Resonance Angiography (MRA) or Computed Tomography Angiography (CTA) provide a sharper, clearer boundary of the lumen and therefore facilitate the segmentation task significantly. Both CTA and MRA currently provide sub-millimeter resolutions that allow for accurate reconstructions of the thoracic aorta, endograft and main branches, such as renal arteries, mesenteric and iliac arteries, etc.

3.1.2 CFD Analysis

Once the geometric model of the aortic endograft and the vessels of interest is created, a discretization of the model into a grid suitable for numerical simulation is needed. Here, it is important to generate a grid that represents accurately both the geometry and the solution field (i.e. velocity and pressure). Some desirable features in the grid-generation process are boundary layer meshing, curvature-based refinement and anisotropic, field-based mesh adaptation techniques [36].

A critical step in the CFD analysis is the boundary condition specification. In this process, one must provide adequate information on flow, pressure and potentially vessel wall dynamics on the boundaries of the geometry. This is an active area of research, and currently the most sophisticated approaches rely on coupling reduced-order mathematical models of the proximal and distal circulation to the inlet(s) and outlets of the model [41, 43]. Typically, a supraceliac waveform mapped to a Womersley velocity profile is prescribed at the inlet face of an abdominal aortic endograft model. This waveform can be obtained either directly from Phase-Contrast Magnetic Resonance Imaging (PC–MRI) techniques or from morphometric measurements [23]. In the case of thoracic aortic endograft modeling, a lumped-parameter heart model representing the interactions between the heart and the thoracic aorta [21] may be utilized on the inlet face of the model. For the outflow boundaries, a powerful and versatile solution consists of coupling a three-element Windkessel lumped parameter model representing the resistance and compliance of the vascular beds that are not physically included in the 3D geometrical model [11, 44]. This approach presents important conceptual advantages:

- It does not rely on the specification of any of the primary blood flow variables (flow or pressure), which are generally not known and are part of the desired solution.
- It avoids potentially serious synchronization issues between flow and pressure waveforms in different parts of the domain. These lumped-parameter outlet conditions adapt naturally to the flow "collected" on each of the outlet faces and calculate a pressure based on the specific downstream model. This pressure is then applied as a weak traction on each of the boundary faces.

Once the process of generating a geometrically-accurate aortic endograft geometric model is finished, and the corresponding computational grid and inflow and outflow boundary conditions are determined, a CFD analysis is performed whereby the Navier–Stokes equations of an incompressible fluid are solved in the domain of interest with the ultimate goal of obtaining a characterization of blood flow velocity and pressure. This analysis is usually very time-consuming since it requires obtaining the solution for velocity and pressure in thousands of time steps for grids that are usually well over one million degrees-of-freedom. Hence, a parallel Finite-Element or Finite-Volume implementation of a solver for the Navier–Stokes equations running in a computer cluster is required in order to bring

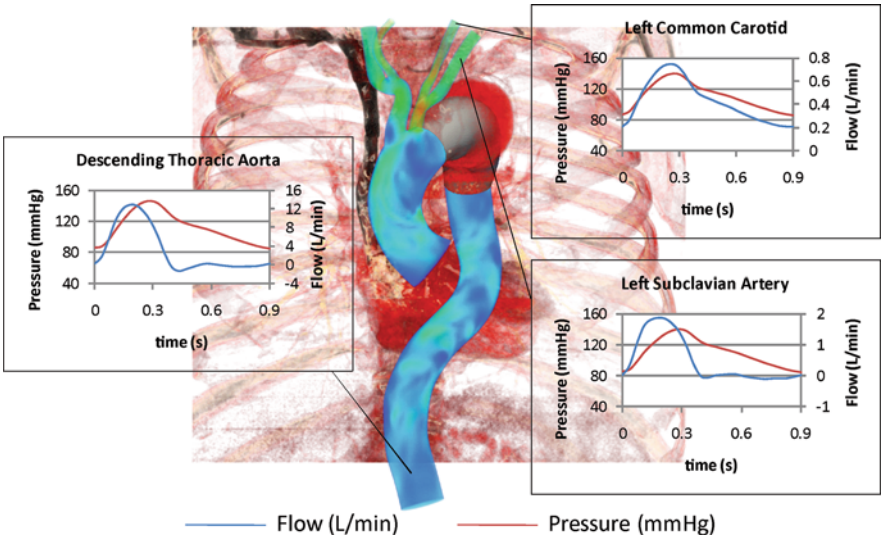

Fig. 9 Flow and pressure waveforms in selected vessels obtained in the CFD analysis of a proximal descending thoracic aortic aneurysm (TAA) model. Note the physiologic range of the waveforms, presenting features such as retrograde flow in the descending aorta during early systole, and forward flow through the cycle in the common carotid artery. Reproduced from Figueroa et al. [9, 10]

the computation time down to the point where the CFD results can be generated in a matter of hours [41].

By choosing a suitable distribution ofi nflow and outflow boundary conditions, it is possible to achieve physiologically-relevant distributions of flow and pressure in the computational model (see Fig.9). The figure shows the pressure and flow waveforms in the descending thoracic aorta, left subclavian artery, and left common carotid artery obtained in the CFD simulations of a proximal descending thoracic aortic aneurysm (TAA) treated with an endograft. The variables defining the hemodynamic state used in the CFD analysis were typical values for volumetric flow and pressure for the ascending thoracic aorta: The mean flow and heart rate is 4.9 L/min and 67 beats per minute, respectively. The aortic systolic, diastolic, and mean pressures were 145, 85, and 111 mmHg, respectively. The figure clearly shows the differences between the descending thoracic aorta and common carotid artery flow waveforms, with forward flow in the carotid artery throughout the cardiac cycle and reversed flow in the descending aorta during diastole, which represent normal physiological variations.

3.1.3 Displacement Force Calculation

Once the CFD results for velocity and pressure in the computer model are obtained, it is possible to investigate the overall effect of the actions of blood flow

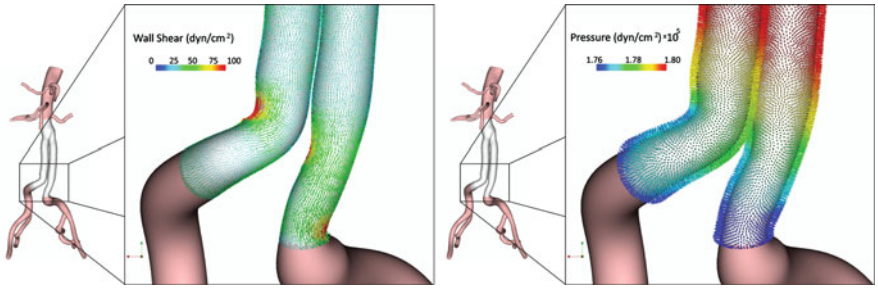

Fig. 10 Wall shear (left) and pressure (right) stresses representing the actions of the blood on the endograft. These stresses are integrated over the surface of the endograft to calculate the total 3D force exerted by the pulsatile flow. Note that the pressure is several orders of magnitude larger than the shear stress. Reproduced from Figueroa et al. [10]

on the endograft. Specifically, the displacement force DF can be obtained by integrating the total traction (i.e. sum of the wall-shear stress and the total normal stress) over the surface of the endograft. Figure10 illustrates how the contribution of the pressure to the total load experienced by the device is several orders of magnitude larger than the wall shear stress contribution. This implies that the pressure of the patient has a much larger impact than the cardiac output on the forces exerted by the blood flow on the device. Therefore, chronic alterations in pressure as a result of hypertension should be watched carefully during the follow-up of the patient.

Contrary to what is often assumed, the endograft displacement force does not act primarily in the longitudinal direction of flow: in situations of significant aneurysm tortuosity the displacement force has important antero-posterior and lateral components (see Fig.11). This example illustrates the power of computational methods towards investigating the loads experienced by endografts in vivo: these techniques make it simple to account for complex, subject-specific geometries of aorta and endograft, and once proper boundary conditions for flow and pressure are obtained to match known patient data, one can easily investigate parameters such as mean and temporal variation of displacement forces, spatial components in the longitudinal, anterior, and lateral directions, etc.

The subject of the example depicted in Fig.11 has a supraceliac aortic flow of 1 L/min, a heart rate of 60 beats per minute, and systolic and diastolic blood pressures of 168 and 92 mmHg, respectively. These conditions result in a pulsatile endograft displacement force ranging from 6.8 N in peak systole and 3.6 N in diastole, with a temporal mean of 5 N. Of this total force, only 28% (1.4 N) is directed in the axial direction. This may have important consequences on the fixation forces that the device must develop in the aortic neck in order to remain attached to the vessel wall.

Other variables than can be easily investigated are the effect on displacement forces of parameters such as endograft diameter and length, aneurysm angulation, graft bifurcation angle, blood pressure, exercise, etc. These variables been have

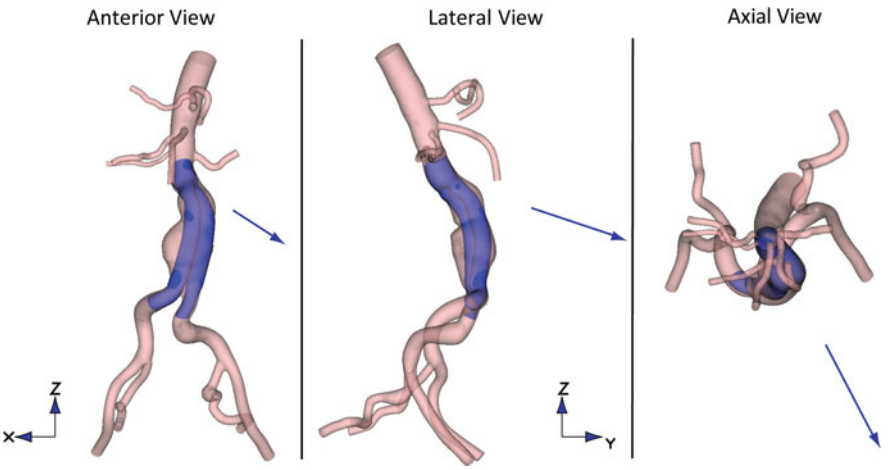

Fig. 11 Anterior, lateral, and axial views of an AAA model with a stent-graft in place. Note the antero-lateral angulation of the endograft, which follows the curved anatomy of the abdominal aorta. The vector of displacement force in drawn to scale in each of the three views

investigated in idealized [22] and patient-specific models [9, 10] of thoracic and abdominal endograft models. Finally, CFD techniques may also provide insight into transport or residence time of thrombogenic agents within the endograft [38].

In the following section, we provide several examples of how computationally determined endograft displacement forces may provide useful insight regarding the hemodynamic conditions experienced by these devices in vivo. We illustrate how these conditions are affected by an array off actors, including curvature, device diameter, blood flow and blood pressure.

3.2 Application Examples

3.2.1 Effect of Curvature on Displacement Forces Acting on Abdominal Endografts

In order to investigate the impact of aortic curvature on the displacement forces experienced by stent-grafts, the computer model depicted in Fig.11 was modified to accommodate the endograft in an almost flat or planar configuration without changing the dimensions of the device. These changes produced a model with a much smaller curvature in the antero-posterior and lateral directions in the aneurysm region (see Fig. 12).

The aortic and branch flow and pressure boundary conditions remained unchanged between the curved and reduced curvature endograft models. The CFD simulations for both models show that there are virtually no differences in the

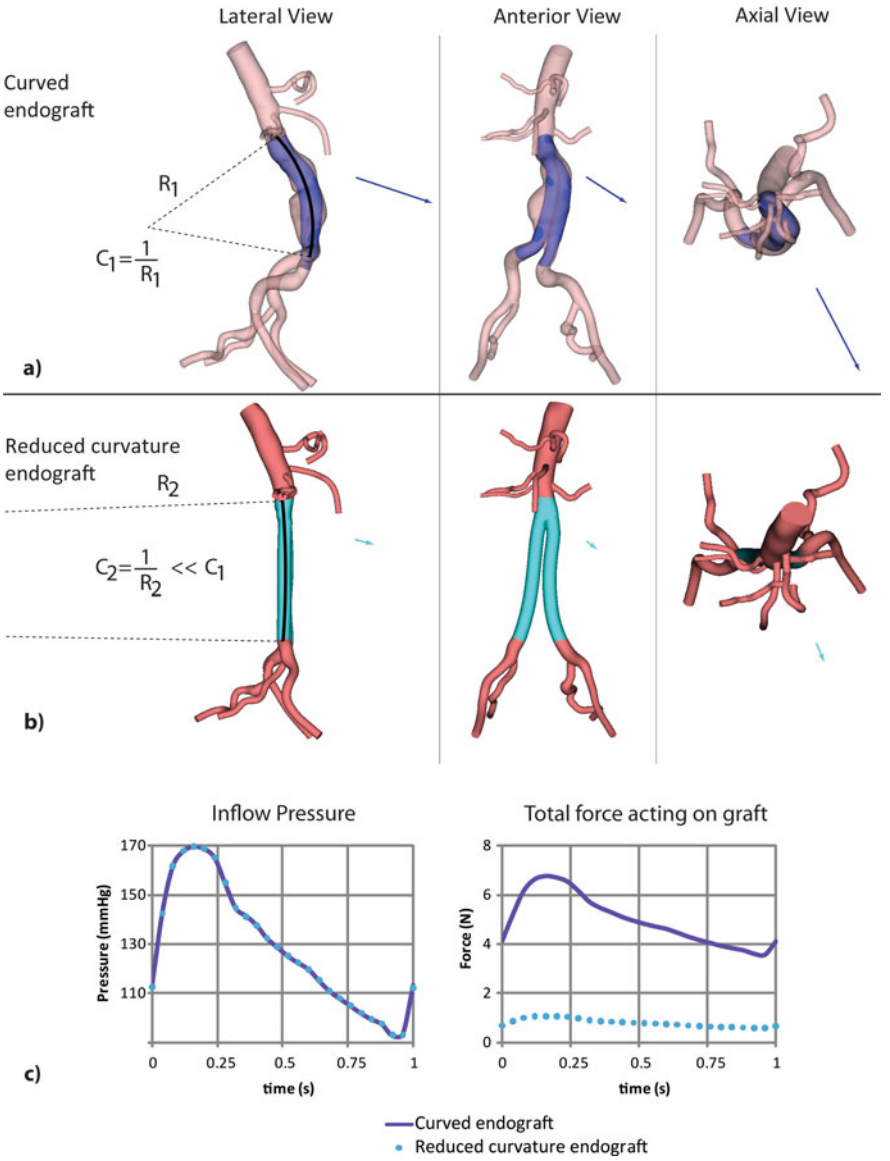

Fig. 12 Lateral, anterior and axial views of the time average of the displacement force acting on the curved endograft model (a) and reduced curvature endograft model (b). The dimensions of the reduced endograft model are identical to those of the curved endograft. Note the reduction in magnitude of the displacement force acting on the endograft as reflected by the size of the arrows. (c) Shows the comparison of the supraceliac and displacement force plots for the two endografts. Note that while the pressures are almost identical, there is a five-fold decrease in pulsatile displacement force (average of 5.01 vs. 0.8 N) in the reduced curvature endograft

Table 1 Total and 3D components of displacement force DF for the curved and reduced curvature endografts

	Curved endograft	Reduced curvature endograft
F_x (lateral) (N)	- 2.22	- 0.29
F_y (anterior) (N)	4.26	0.72
F_z (axial) (N)	- 1.42	- 0.24
Total force (N)	5.01	0.81
% Downward	28.35	29.54

aortic pressure between the two models: this indicates that local changes in curvature or tortuosity do not significantly affect the pressure field in the aorta unless they are accompanied by geometric changes such as narrowing (stenosis) or enlargement sections that may significantly alter the flow field.

The differences in the total displacement force between the two models are however, significant: the temporal average of the total displacement force in the planar endograft was reduced by more than five-fold from 5 to 0.8 N compared to the normally positioned curved endograft. The total and 3D components of the displacement force for both models are given in Table 1.

In both the curved and reduced curvature endografts the largest components of the force was acting in the anterior direction, which can be explained by the angulation of the neck of the abdominal aorta, directing the blood flow to impinge against the anterior face of the endograft and therefore increasing the dynamic component of the pressure on that surface.

3.2.2 Effect of Increased Pressure and Flow on Displacement Forces Acting on Thoracic Endografts

Blood flow and pressure can vary significantly during the course of the day in response to changes in activity level, and chronically due to processes such as hypertension and physical training. It is therefore important to understand the effects of altered flow and pressure on the forces experienced by endografts. We investigate these effects using a patient-specific model of a thoracic aortic endograft. The endograft consists of three modules with an average diameter of 36 mm spanning a length of approximately 30 cm used to repair a mid-descending thoracic aortic aneurysm (TAA) (see Fig. 13).

The variables defining the hemodynamic state used in the CFD analysis represented typical values for volumetric flow and pressure for the thoracic aorta. The mean flow and heart rate were 4.9 L/min and 67 bpm, respectively. The aortic systolic, diastolic, and mean pressures were 145, 85, and 111 mmHg, respectively (pressure pulse of 60 mmHg). Calculation of the endograft displacement force DF produced a vector with significantly larger mean (21.7 N), peak systolic (27.8 N) and end-diastolic (16.7 N) values than those typically found on abdominal endografts. Figure 13 shows the anterior, lateral, and axial views of the thoracic model and the DF vector (blue arrow) resulting from the baseline flow and pressure

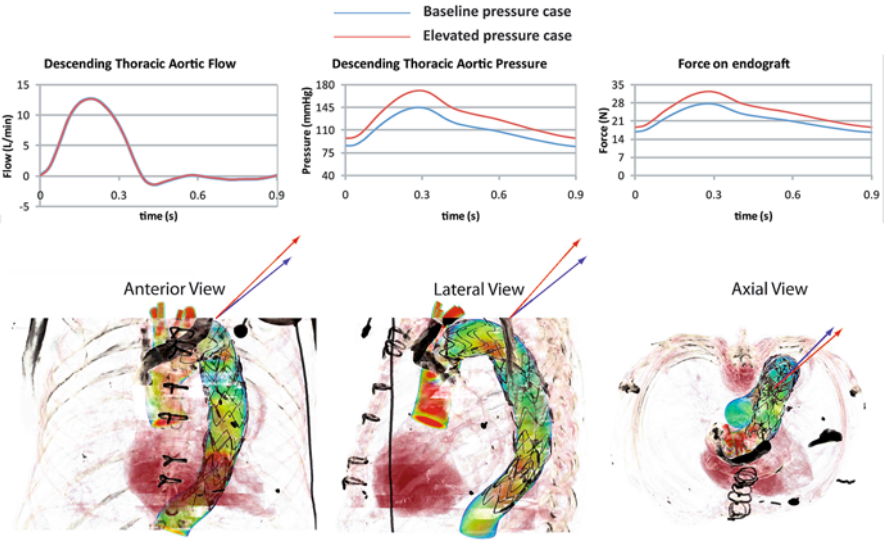

Fig. 13 Flow and pressure waves with pulsatile DF for the baseline pressure (blue plots) and the elevated pressure (red plots) simulations. The images compare the orientation of the DF vectors for the baseline pressure (blue arrows) and the elevated pressure (red arrows) scenarios in the anterior, lateral, and axial views. Modified from [9]

conditions given above. Note that the orientation of the DF vector follows the curvature of the endograft and shows a significant component (10.8 N) acting in the craniad direction. The waveforms corresponding to baseline conditions of thoracic aortic flow, descending aortic pressure, and pulsatile DF are given in blue.

We investigated a situation of moderate increase in blood pressure (see red waveforms in Fig. 13) with no changes in cardiac output. The elevated pressure waveform had a mean value of 130 mmHg, with a systolic peak of 171 mmHg, a diastolic minimum of 97 mmHg, and a pulse pressure of 74 mmHg. Thus, this represented an increase of 16.5% in mean pressure with respect to be baseline conditions. The DF vector, shown in red arrows in Fig.13, had larger mean (25 N), peak systolic (32.5 N), and diastolic (22.6 N) values than in the baseline pressure conditions. This indicates that the increase in mean DF was approximately linearly proportional to the increase in mean pressure over the range of pressure considered. Furthermore, the increase in pulse pressure resulted in a significant change in the orientation of the DF vector. Table 2 compares the axial (craniad) and sideways components of the baseline pressure conditions to the values for the elevated pressure simulation. The greatest increase was in the axial component (37%), whereas the increase in the sideways component was only 7%, which can be explained by the increased acceleration of blood due to the 14 mmHg higher pulse pressure. The blood was therefore pushed against the outer curve of the graft more vigorously than before, which resulted in the larger craniad component of the DF vector.

Table 2 Axial component, transverse component and total mean displacement force DF for the baseline pressure and elevated pressure conditions

	Baseline pressure	Elevated pressure	Increase (%)
Axial component (craniad) (N)	10.8	14.8	37
Transverse component (N)	18.8	20.1	7
Total force (N)	21.7	25	15

We then investigated the impact ofi ncreased flow on the DF experienced by the endograft. We considered a situation ofl ight exercise corresponding to a 2.5-fold increase in cardiac output from 4.9 to 12.24 L/min, and 50% increase in heart rate from 67 to 100 bpm. We adjusted the outflow branches boundary conditions to represent realistic changes in thoracic pressure during moderate exercise: 55% increase in pulse pressure from 60 to 93 mmHg; almost no change in diastolic pressure resulting in an increase in mean pressure of 12.5% from 112 to 126 mmHg. These changes of 50% increase in flow rate and the corresponding 12.5% increase in mean blood pressure resulted in a modest 10% increase in the mean DF experienced by the endograft. This indicates that the changes in DF are influenced mostly by changes in blood pressure resulting from the increased level of physical activity. Furthermore, the orientation of the DF vector remained relatively unchanged with respect to the baseline conditions.

3.2.3 Correlation Between Endograft Motion and Post-operative Displacement Forces

To date, there has not been a consistent definition of endograft migration. Migration has been variously defined using an arbitrarily selected distance, such as 5 or 10 mm, or in some cases as an endograft movement that results in the need for a secondary intervention [27, 40, 48]. Most clinical studies quantifying endograft movement have relied on one-dimensional [4,34, 48] or two-dimensional techniques [33] (see Fig. 14). Measurements have included axial or centerline distances from the renal arteries or superior mesenteric artery to the first appearance of the endograft or to the appearance of the complete fabric-stent ring. However, change in endograft position is actually a complex process in three-dimensional space. Quantification of three-dimensional positional changes of the endograft over time is challenging due to its geometric complexity, the need to co-register two different images in space, and the non-uniform movement of the device, since some parts of the endograft may experience a significant movement while others remain stationary.

We have recently proposed a methodology to quantify the three-dimensional displacement of an endograft based on tracking the position of the centroid of the device over time. The endograft centroid is co-registered in two images, typically a baseline post-operative scan and a follow-up scan, using the center point of the inferior edge of the L3 vertebra as anatomic landmark (yellow dot) (Fig.15).

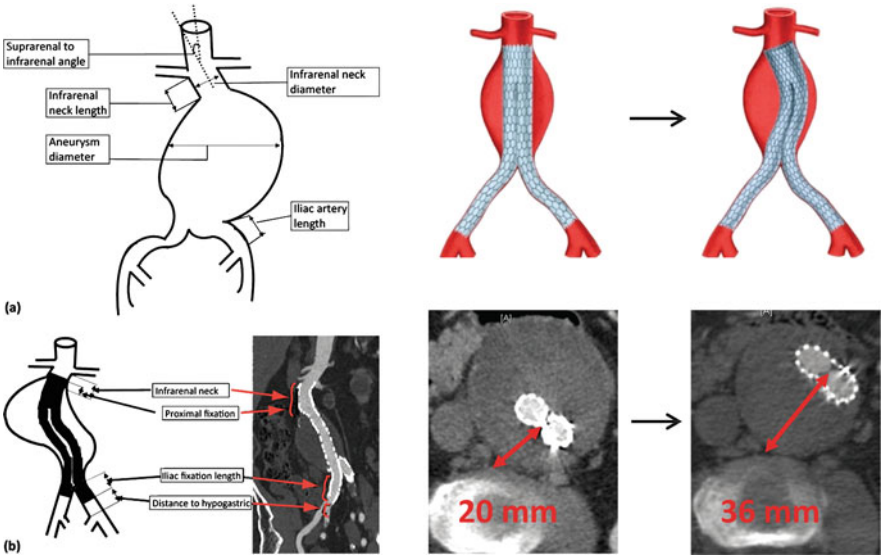

Fig. 14 Studies quantifying endograft movement using 1 or 2D techniques. Left Benharash et al. [4] have measured the longitudinal endograft movement with respect to the position of the renal arteries. Right [33] have measured the transverse movement of the endograft with respect to an anatomic landmark in the spine

The distance between the co-registered centroid in the baseline scan (red dot) and follow-up scan (green dot) characterizes the three-dimensional movement of the endograft, which has components in the anterior, lateral, and axial directions.

Once the movement between baseline and follow-up scans is obtained, we investigated the correlation between the orientation of the post-operative endograft displacement force vector and the direction of endograft movement. The metric of the correlation is given by the cosine of the angle between the displacement force and the movement vectors [11]. This correlation can be helpful to predict, using post-operative or even pre-operative imaged data of a patient, the direction in which the endograft is likely to move.

Figure 16 shows the anterior and lateral views of the computed post-operative displacement force vector (red arrows) and measured movement vector (yellow arrows) between baseline and follow-up scans for 5 AAA patients with significant endograft movement that in general resulted in the need for a secondary procedure. Four out the five patients (patient 1, 2, 4 and 5) had late device migration (average time to secondary procedure of 3.3 years). Patient 3 however required a secondary procedure after only 8 months to correct a left iliac type I endoleak.

With the exception of patient 3 who showed a very small correlation between displacement force and displacement vectors, the correlation between the orientation of the post-operative displacement force vector and the movement vector was rather high for the patients with shorter follow-up intervals (average correlation metric of 0.46). This correlation could be further improved iff actors such as

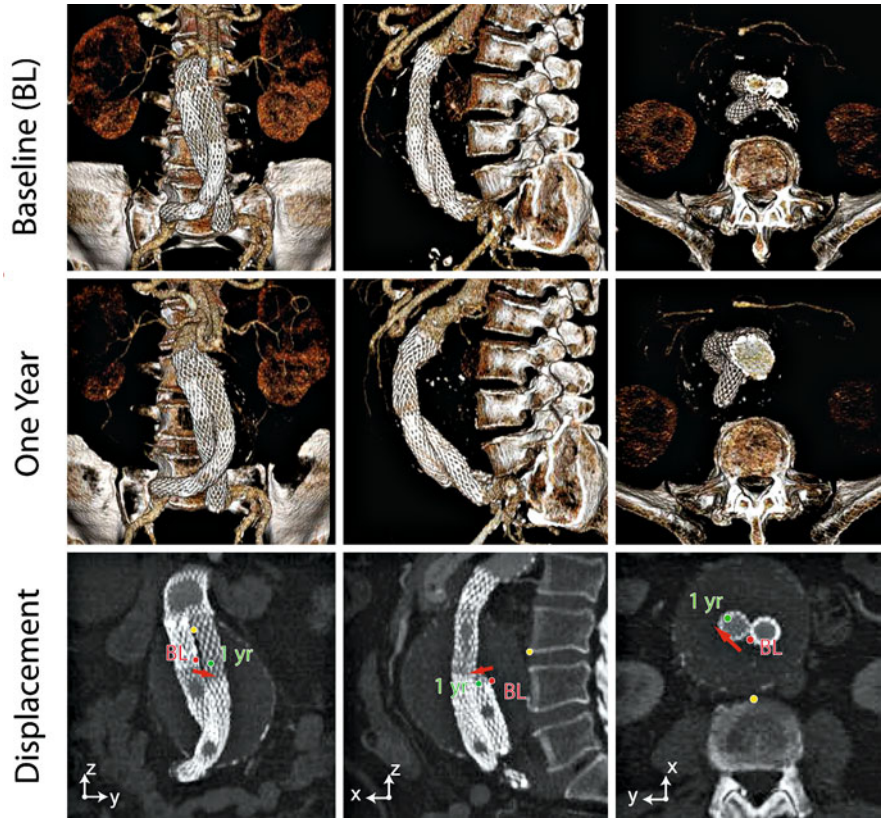

Fig. 15 3D analysis of the endograft centroid movement between a baseline post-operative state (top row), and a one-year follow-up state (middle row). The endograft centroid moves primarily in the antero-lateral direction (17.6 mm in the xy plane), and also in the axial direction (3 mm in z). Adapted from Figueroa et al. [11]

the position of the endograft within the aneurysm sac are considered. For instance, patient 3 has the endograft leaning directly against the anterior wall of the aneurysm. Therefore, even though the post-operative displacement force acts primarily in the posterior-anterior direction, the endograft is unlikely to move in that direction due to the constraint provided by the aneurysm wall.

4 Summary and Conclusions

In this article, we have provided an overview of the state of the art of the Computational Fluid Dynamics tools used to characterize the hemodynamics in patients treated with abdominal and thoracic stent-grafts and of the most common complications experienced by these devices. Computational modeling of patient-

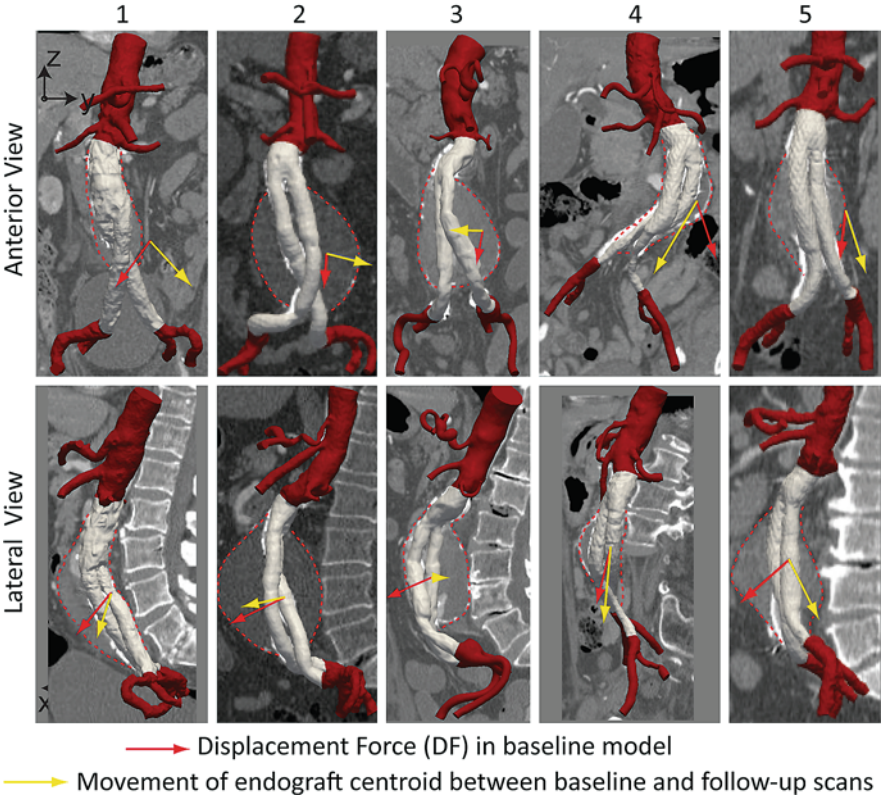

Fig. 16 Displacement force (red arrows) and endograft centroid movement (yellow arrows) vectors in the anterior and lateral views for the 5 patients who experienced abdominal endograft migration. Relative sizes of arrows reflect magnitude of the vectors. Adapted from Figueroa et al. [11]

specific endograft dynamics provides an unprecedented insight into the in vivo hemodynamic conditions experienced by these devices. These techniques have relied on recent progress in the areas of diagnostic medical imaging, image processing, computational fluid dynamics algorithms for fast, highly scalable parallel iterative solvers, and finally, computer hardware [41]. Computer modeling techniques, although still in need off urther improvements, provide a powerful and versatile tool to test and analyze numerous loading conditions and design solutions: for instance, it is easy to investigate alterations in the loading conditions experienced by endografts following changes in blood pressure and blood flow and to virtually modify the size of the various components of the device. Figure 17 provides a schematic representation of how computational, experimental, and clinical tools can be combined to better understand and monitor the performance of aortic stent-grafts. Part a) represents the CFD analysis performed on the geometry given by the aneurysm and the device and provides the distribution of

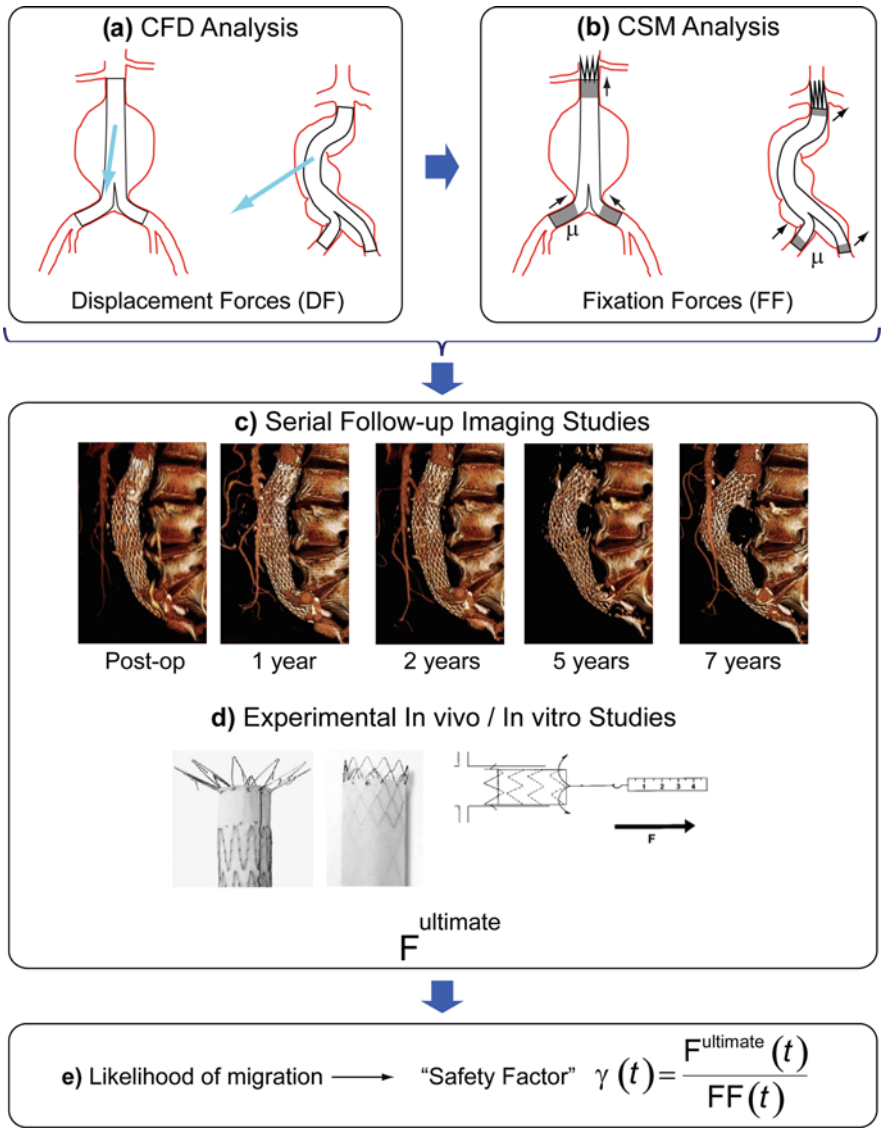

Fig. 17 A computational framework where a combination of computational, clinical, imaging, and experimental tools are used to evaluate the performance of abdominal stent-grafts in vivo

loads or displacement forces DF experienced by the endograft. In part b), a CSM analysis evaluates the fixation of the device to the vessel wall. The device is subjected to the displacement forces DF obtained in the CFD analysis. The fixation forces FF depend on the fixation characteristics of the device, represented by the coefficient l in the figure. Part c) represents the clinical evidence gathered via longitudinal imaging studies of the performance of a given device implanted in a

patient: This evidence may be used to define areas of attachment between device and aorta, to quantify the amount ofi ntra-luminal thrombus and its potential constraining effect on the endograft, and to assess the disease state of the vessel wall in terms of atherosclerotic plaque and calcifications. These are all parameters that provide useful information for the CSM analysis depicted in part b). Finally, in part d) experimental in vivo and in vitro data provide direct measurement of the fixation response of a given device as a function of oversizing, the characteristics of the luminal surface, etc. Information obtained from c) and d) can then be used to estimate the ultimate fixation force that a given device can provide in a specific configuration. Once this ultimate fixation response is evaluated, a likelihood of migration for a given device on a given patient can be estimated by the "safety factor" γ defined as the ratio between the ultimate fixation force the device is able to provide and the actual fixation force.

The paradigm of "virtual prototyping" that has been extensively applied for quite some time in industries such as the automotive and the aeronautical is now beginning to be used in the medical device industry as well. The development and application of new computational and imaging tools and the combination of these tools with clinical and experimental data will further improve the design of devices and will ultimately result in improved patient care and reduced costs.

Acknowledgments This research was supported by the National Institutes of Health (Grants P50 HL083800, and 1 RC1 EB011443-01) and the National Science Foundation (Grant CNS-0619926).

References

1. Amblard, A., Berre, H.W.L., Bou-Said, B., Brunet, M.: Analysis of type I endoleaks in a stented abdominal aortic aneurysm. Med. Eng. Phys. 31(1), 27–33 (2009)
2. Arko, F.R., Heikkinen, M., Lee, E.S., Bass, A., Alsac, J.M., Zarins, C.K.: Iliac fixation length and resistance to in vivo stent-graft displacement. J. Vasc. Surg. 41(4), 664–670 (2005)
3. Baum, R.A., Cope, C., Fairman, R.M., Carpenter, J.P.: Translumbar embolization of type 2 endoleaks after endovascular repair of abdominal aortic aneurysms. J. Vasc. Interv. Radiol. 12(1), 111–116 (2001)
4. Benharash, P., Lee, J.T., Abilez, O.J., Crabtree, T., Bloch, D.A., Zarins, C.K.: Iliac fixation inhibits migration of both suprarenal and infrarenal aortic endografts. J. Vasc. Surg. 45(2), 250–257 (2007)
5. Brewster, D.C., Cronenwett, J.L., Hallett, J.W., Johnston, K.W., Krupski, W.C., Matsumura, J.S.: Guidelines for the treatment of abdominal aortic aneurysms—Report of a subcommittee of the joint council of the American association for vascular surgery and society for vascular surgery. J. Vasc. Surg. 37(5), 1106–1117 (2003)
6. Conners, M.S., Sternbergh, W.C., Carter, G., Tonnessen, B.H., Yoselevitz, M., Money, S.R.: Endograft migration one to four years after endovascular abdominal aortic aneurysm repair with the AneuRx device: a cautionary note. J. Vasc. Surg. 36(3), 476–482 (2002)
7. Dalman, R.L., Tedesco, M.M., Myers, J., Taylor, C.A.: AAA disease—mechanism, stratification, and treatment. In: Tilson, M.D., Kuivaniemi, H., Upchurch, G.R. (eds.) Abdominal Aortic Aneurysm: Genetics, Pathophysiology and Molecular Biology, vol. 1085, pp. 92–109. Blackwell Publishing, Oxford (2006)

8. De Bruin, J.L., Baas, A.F., Buth, J., Prinssen, M., Verhoeven, E.L.G., Cuypers, P.W.M., van Sambeek, M., Balm, R., Grobbee, D.E., Blankensteijn, J.D., Grp, D.S.: Long-Term Outcome of Open or endovascular repair of abdominal aortic aneurysm. N. Engl. J. Med. 362(20), 1881–1889 (2010)
9. Figueroa, C.A., Taylor, C.A., Chiou, A.J., Yeh, V., Zarins, C.K.: Magnitude and direction of pulsatile displacement forces acting on thoracic aortic endografts. J. Endovasc. Ther.16(3), 350–358 (2009)
10. Figueroa, C.A., Taylor, C.A., Yeh, V., Chiou, A.J., Zarins, C.K.: Effect of curvature on displacement forces acting on aortic endografts: a 3-dimensional computational analysis. J. Endovasc. Ther. 16(3), 284–294 (2009)
11. Figueroa, C.A., Taylor, C.A., Yeh, V., Chiou, A.J., Gorrepati, M.L., Zarins, C.K.: Preliminary 3D computational analysis of the relationship between aortic displacement force and direction of endograft movement. J. Vasc. Surg. 51(6), 1488–1497 (2010)
12. Fleming, C., Whitlock, E.P., Bell, T.L., Lederle, F.A.: Screening for abdominal aortic aneurysm: a best-evidence systematic review for the US preventive services task force. Ann. Intern. Med. 142(3), 203–211 (2005)
13. Fulton, J.J., Farber, M.A., Sanchez, L.A., Godshall, C.J., Marston, W.A., Mendes, R., Rubin, B.G., Sicard, G.A., Keagy, B.A.: Effect of challenging neck anatomy on mid-term migration rates in AneuRx endografts. J. Vasc. Surg. 44(5), 932–937 (2006)
14. Gillum, R.F.: Epidemiology of aortic-aneurysm in the United-States. J. Clin. Epidemiol. 48(11), 1289–1298 (1995)
15. Greenhalgh, R.M., Brown, L.C., Kwong, G.P.S., Powell, J.T., Thompson, S.G.: Comparison of endovascular aneurysm repair with open repair in patients with abdominal aortic aneurysm (EVAR trial 1), 30-day operative mortality results: randomised controlled trial. Lancet 364(9437), 843–848 (2004)
16. Greenhalgh, R.M., Brown, L.C., Epstein, D., Kwong, G.P.S., Powell, J.T., Sculpher, M.J., Thompson, S.G., Participants, E.T.: Endovascular aneurysm repair versus open repair in patients with abdominal aortic aneurysm (EVAR trial 1): randomised controlled trial. Lancet 365(9478), 2179–2186 (2005)
17. Heikkinen, M.A., Alsac, J.M., Arko, F.R., Metsanoja, R., Zvaigzne, A., Zarins, C.K.: The importance ofi liac fixation in prevention of stent graft migration. J. Vasc. Surg. 43(6), 1130–1137 (2006)
18. Heller, J.A., Weinberg, A., Arons, R., Krishnasastry, K.V., Lyon, R.T., Deitch, J.S., Schulick, A.H., Bush, H.L., Kent, K.C.: Two decades of abdominal aortic aneurysm repair: have we made any progress? J. Vasc. Surg.32(6), 1091–1098 (2000)
19. Hobo, R., Kievit, J., Leurs, L.J., Buth, J., Collaborators, E.: Influence of severe infrarenal aortic neck angulation on complications at the proximal neck following endovascular AAA repair: a eurostar study. J. Endovasc. Ther.14(1), 1–11 (2007)
20. Howell, B.A., Kim, T., Cheer, A., Dwyer, H., Saloner, D., Chuter, T.A.M.: Computational fluid dynamics within bifurcated abdominal aortic stent-Grafts. J. Endovasc. Ther. 14(2), 138–143 (2007)
21. Kim, H.J., Vignon-Clementel, I.E., Figueroa, C.A., LaDisa, J.F., Jansen, K.E., Feinstein, J.A., Taylor, C.A.: On coupling a lumped parameter heart model and a three-dimensional finite element aorta model. Ann. Biomed. Eng. 37(11), 2153–2169 (2009)
22. Kleinstreuer, C., Li, Z.: Analysis of biomechanical factors affecting stent-graft migration in an abdominal aortic aneurysm model. J. Biomech. 39(12), 2264–2273 (2006)
23. Les, A., Yeung, J., Schultz, G., Herfkens, R., Dalman, R., Taylor, C.: Supraceliac and infrarenal aortic flow in patients with abdominal aortic aneurysms: mean flows, waveforms, and allometric scaling relationships. Cardiovasc. Eng. Technol.1(1), 39–51 (2010)
24. Li, Z., Kleinstreuer, C., Farber, M.: Computational analysis of biomechanical contributors to endovascular graft failure. Biomech. Model. Mechanobiol.4(4), 221–234 (2005)
25. Malina, M., Lindblad, B., Ivancev, K., Lindh, M., Malina, J., Brunkwall, J.: Endovascular AAA exclusion: Will stents with hooks and barbs prevent stent-graft migration? J. Endovasc. Surg. 5(4), 310–317 (1998)

26. Malladi, R., Sethian, J.A., Vemuri, B.C.: Shape modeling with front propagation—a level set approach. IEEE Trans. Pattern Anal. Mach. Intell. 17(2), 158–175 (1995)
27. Matsumura, J.S., Brewster, D.C., Makaroun, M.S., Naftel, D.C., Excluder Bifurcated, E.: A multicenter controlled clinical trial of open versus endovascular treatment of abdominal aortic aneurysm. J. Vasc. Surg. 37(2), 262–271 (2003)
28. Molony, D.S., Callanan, A., Morris, L.G., Doyle, B.J., Walsh, M.T., McGloughlin, T.M.: Geometrical enhancements for abdominal aortic stent-grafts. J. Endovasc. Ther.15(5), 518–529 (2008)
29. Morris, L., Delassus, P., Walsh, M., McGloughlin, T.: A mathematical model to predict the in vivo pulsatile drag forces acting on bifurcated stent grafts used in endovascular treatment of abdominal aortic aneurysms (AAA). J. Biomech. 37(7), 1087–1095 (2004)
30. Murphy, E.H., Johnson, E.D., Arko, F.R.: Device-specific resistance to in vivo displacement of stent-grafts implanted with maximum iliac fixation. J. Endovasc. Ther.14(4), 585–592 (2007)
31. Nabi, D., Murphy, E.H., Pak, J., Zarins, C.K.: Open surgical repair after failed endovascular aneurysm repair: is endograft removal necessary? J. Vasc. Surg. 50(4), 714–721 (2009)
32. Parodi, J.C., Barone, A., Piraino, R., Schonholz, C.: Endovascular treatment of abdominal aortic aneurysms: lessons learned. J. Endovasc. Surg. 4(2), 102–110 (1997)
33. Rafii, B.Y., Abilez, O.J., Benharash, P., Zarins, C.K.: Lateral movement of endografts within the aneurysm sac is an indicator of stent-graft instability. J. Endovasc. Ther.15(3), 335–343 (2008)
34. Resch, T., Ivancev, K., Brunkwall, J., Nyman, U., Malina, M., Lindblad, B.: Distal migration of stent-grafts after endovascular repair of abdominal aortic aneurysms. J. Vasc. Interv. Radiol. 10(3), 257–264 (1999)
35. Resch, T., Malina, M., Lindblad, B., Malina, J., Brunkwall, J., Ivancev, K.: The impact of stent design on proximal stent-graft fixation in the abdominal aorta: an experimental study. Eur. J. Vasc. Endovasc. Surg. 20(2), 190–195 (2000)
36. Sahni, O., Muller, J., Jansen, K.E., Shephard, M.S., Taylor, C.A.: Efficient anisotropic adaptive discretization of the cardiovascular system. Comput. Methods Appl. Mech. Eng. 195(41–43), 5634–5655 (2006)
37. Sampaio, S.M., Panneton, J.M., Mozes, G., Andrews, J.C., Noel, A.A., Kalra, M., Bower, T.C., Cherry, K.J., Sullivan, T.M., Gloviczki, P.: AneuRx device migration: incidence, risk factors, and consequences. Ann. Vasc. Surg.19(2), 178–185 (2005)
38. Shadden, S.C., Taylor, C.A.: Characterization of coherent structures in the cardiovascular system. Ann. Biomed. Eng. 36(7), 1152–1162 (2008)
39. Sternbergh, W.C., Carter, G., York, J.W., Yoselevitz, M., Money, S.R.: Aortic neck angulation predicts adverse outcome with endovascular abdominal aortic aneurysm repair. J. Vasc. Surg. 35(3), 482–486 (2002)
40. Sternbergh, W.C., Money, S.R., Greenberg, R.K., Chuter, T.A.M., Zenith, I.: Influence of endograft oversizing on device migration, endoleak, aneurysm shrinkage, and aortic neck dilation: results from the Zenith multicenter trial. J. Vasc. Surg.39(1), 20–26 (2004)
41. Taylor, C.A., Figueroa, C.A.: Patient-specific modeling of cardiovascular mechanics. Annu. Rev. Biomed. Eng. 11, 109–134 (2009)
42. Veith, F.J., Baum, R.A., Ohki, T., Amor, M., Adiseshiah, M., Blankensteijn, J.D., Buth, J., Chuter, T.A.M., Fairman, R.M., Gilling-Smith, G., Harris, P.L., Hodgson, K.J., Hopkinson, B.R., Ivancev, K., Katzen, B.T., Lawrence-Brown, M., Meier, G.H., Malina, M., Makaroun, M.S., Parodi, J.C., Richter, G.M., Rubin, G.D., Stelter, W.J., White, G.H., White, R.A., Wisselink, W., Zarins, C.K.: Nature and significance of endoleaks and endotension: summary of opinions expressed at an international conference. J. Vasc. Surg. 35(5), 1029–1035 (2002)
43. Vignon-Clementel, I.E., Figueroa, C.A., Jansen, K.E., Taylor, C.A.: Outflow boundary conditions for three-dimensional finite element modeling of blood flow and pressure in arteries. Comput. Methods Appl. Mech. Eng.195(29–32), 3776–3796 (2006)

44. Vignon-Clementel, I.E., Figueroa, C.A., Jansen, K.E., Taylor, C.A.: Outflow boundary conditions for 3D simulations of non-periodic blood flow and pressure fields in deformable arteries. Comput. Methods Biomech. Biomed. Eng.13(5), 625–640 (2010)
45. Wang, K.C., Dutton, R.W., Taylor, C.A.: Improving geometric model construction for blood flow modeling—geometric image segmentation and image-based model construction for computational hemodynamics. IEEE Eng. Med. Biol. Mag. 18(6), 33–39 (1999)
46. White, G.H., Yu, W.J., May, J., Chaufour, X., Stephen, M.S.: Endoleak as a complication of endoluminal grafting of abdominal aortic aneurysms: classification, incidence, diagnosis, and management. J. Endovasc. Surg. 4(2), 152–168 (1997)
47. Yushkevich, P.A., Piven, J., Hazlett, H.C., Smith, R.G., Ho, S., Gee, J.C., Gerig, G.: User-guided 3D active contour segmentation of anatomical structures: significantly improved efficiency and reliability. Neuroimage31(3), 1116–1128 (2006)
48. Zarins, C.K., Bloch, D.A., Crabtree, T., Matsumoto, A.H., White, R.A., Fogarty, T.J.: Stent graft migration after endovascular aneurysm repair: importance of proximal fixation. J. Vasc. Surg. 38(6), 1264–1272 (2003)
49. Zarins, C.K., Gewertz, B.L.: Atlas of vascular surgery. Elsevier, Philadelphia (2005)